Multiple Functionality in Nanotube Transistors

François Léonard¹ and J. Tersoff²

¹ Sandia National Laboratories, MS 9161, Livermore, CA 94551,

USA.

²IBM Research Division, T. J. Watson Research Center, P.O. Box 218, Yorktown Heights, NY 10598, USA. (October 30, 2018)

Calculations of quantum transport in a carbon nanotube transistor show that such a device offers unique functionality. It can operate as a ballistic field-effect transistor, with excellent characteristics even when scaled to 10 nm dimensions. At larger gate voltages, channel inversion leads to resonant tunneling through an electrostatically defined nanoscale quantum dot. Thus the transistor becomes a gated resonant-tunneling device, with negative differential resistance at a tunable threshold. For the dimensions considered here, the device operates in the Coulomb blockade regime, even at room temperature.

In the quest for nanoscale devices, carbon nanotubes (NTs) [1] have emerged as a promising material with unique electronic and mechanical properties. Theoretical studies of NT devices have focused primarily on two-terminal devices [2–8]. However, practical device architectures generally require three-terminal devices; and current technology is built primarily around field-effect transistors (FETs). A number of groups have fabricated NT-based FETs [9–12], and have demonstrated promising transistor functionality. The devices realized experimentally typically have dimensions in the micron range. However, the real promise of NTs lies in the possibility of nanoscale devices. At this size scale, new effects can become important, creating new problems but also new opportunities.

Here we show that a nanoscale NT FET offers unique functionality that goes beyond any existing device. The device geometry we consider, shown in Fig. 1, is a straightforward idealization of that already used for NT FETs [9,10], and does not require doping [2,5] or structural modification [13] of the nanotube. Our calculations show that, for a 10 nm channel length, the device operates as an excellent ballistic transistor, with current saturation at high bias. In addition, the gate voltage can be used to drive the channel into inversion, defining a nanoscale "quantum dot". Tunneling through a state localized in the dot gives strong negative differential resistance, even at room temperature. The FET can thus operate as a *gated* resonant tunneling device. This approach lifts one of the major limitations of resonant tunneling diodes — the resonance occurs at a sourcedrain voltage that can be directly controlled via the gate voltage [14].

As illustrated in Fig. 1, the device consists of a single-wall, semiconducting carbon NT. It is embedded in metal contacts on either side, defining the source and drain. Between the source and drain electrodes, an insulating dielectric surrounds the NT up to a radius of 10 nm. A

cylindrical gate of radius 10 nm wraps the dielectric and serves to control the device behavior. In our calculations, the NT and the metals are separated by a van der Waals distance of 0.3 nm. (The insulator has dielectric constant $\varepsilon = 3.9$, as for SiO₂, and it is also separated from the tube by 0.3 nm.)

We treat a zigzag NT of index (17.0), which has radius 0.66 nm and band gap 0.55 eV. The qualitative aspects of our results also apply to other semiconducting NTs. We use a tight-binding Hamiltonian with one π orbital per carbon atom and a nearest-neighbor matrix element of 2.5 eV [15]. The metal Fermi level is chosen to be 1 eV below the NT midgap. (For the NT midgap 4.5 eV below the vacuum level [16], this corresponds to a metal workfunction of 5.5 eV, roughly that of Au and Pt.)

We first examine the conductance of the device at low source-drain voltage, as the gate voltage is varied. For a given gate voltage, we obtain the zero-bias conductance from [17]

$$G = \frac{4e^2}{h} \int P(E) \left[-\frac{\partial f(E)}{\partial E} \right] dE , \qquad (1)$$

where the energy E is relative to the Fermi level, P(E) is the electron transmission probability across the device at energy E, and f(E) is the Fermi function. We calculate P(E) using the quantum-transport procedure of Ref. [17], which requires the electrostatic potential $\Phi(z)$ along the NT. (Our device is much smaller than observed scattering lengths [18], so there is no need to include scattering other than reflection by the device itself.) The NT device is divided into three regions: two semi-infinite "leads", and a "device region", which is 18.3 nm in length here unless otherwise specified. Within the scattering region we use the full self-consistent potential $\Phi(z)$. The potentials in the leads are taken as constant, and equal to the potentials at the boundaries of the scattering region.

To obtain the self-consistent potential, as in Ref. [5] we start from a charge $\sigma(z)$, and obtain $\Phi(z)$ by solv-

ing Poisson's equation with boundary conditions set by the source, drain, and gate voltages, with the dielectric. The electronic charge $\sigma(z)$ is re-calculated using $\Phi(z)$, and the procedure is iterated to self-consistency. (Thus charge transfer and energy alignment between NT and metal electrode is included self-consistently.) To calculate $\sigma(z)$, the "scattering region" is periodically repeated, the diagonal elements of the Hamiltonian are shifted by $-e\Phi(z)$, the local density of states on each atomic site is obtained by direct diagonalization of the Hamiltonian, and the charge on each site is given by integration of the product of the local density of states and the Fermi function. (Modifications to include Coulomb blockade effects are discussed below.) The charge associated with a "ring" of atoms is approximated as uniformly distributed over a length 0.07 nm of the NT cylinder and over a radial thickness of 0.1 nm. The potential is not sensitive to the details of this approximation [5]. Because the NT does not form covalent bonds with the metal or dielectric, we focus on the limit of weak metal-NT coupling. Then the matrix elements of the NT Hamiltonian are unaffected by the metal, but charge transfer between metal and NT (and the resulting electrostatic potential) must still be included.

Figure 2a shows the calculated conductance as a function of gate voltage V_G . Three distinct regimes are seen. At low V_G (region I in Fig. 2a), the device exhibits high conductance, while at higher V_G (region II in Fig. 2a) the conductance drops to practically zero. These correspond to the "on" and "off" states of a FET. In addition, there is a third regime (region III of Fig. 2a) which has no analog in conventional transistors. Here the conductance rises sharply with V_G , and then drops to practically zero again.

This behavior can be understood in terms of the band diagram of the device in the respective regimes. Figure 2b shows the band diagram at low V_G . The Fermi level falls below the valence-band edge of the NT, due to the high metal workfunction, so there is substantial free charge (as holes) in the leads. There is essentially no barrier to hole transport through the channel of the device, explaining the very high conductance. (The highest conductance possible is 1 on this scale, corresponding to perfect transmission through the device.)

With increasing V_G , the bands in the channel are pulled down in energy, Fig. 2c. This creates a substantial energy barrier for transport of holes across the depleted channel, turning off the current. The gate voltage required to turn off the device could be reduced by increasing the channel length or reducing the gate radius.

With increasing gate voltage V_G , conduction-band states are electrostatically pulled down into the band gap. The resulting quantum confinement defines a "quantum dot" with localized states, Fig. 2d. For sufficiently large V_G , the lowest energy level of the quantum dot drops below the asymptotic valence band edge. Electrons (or equivalently, holes) can then tunnel through the quantum dot, giving a sharp rise in conductance. At this point the quantum-dot level is a resonance, rather than truly localized. The conductance is maximal when the localized level reaches the Fermi level. Once the level drops more than $\sim k_B T$ below the Fermi level, there are exponentially few holes at the energy of the localized level, and the conductance drops sharply. This resonant tunneling also leads to strong negative differential resistance, as described below. Moreover, in principle one could design a transistor with sharper turn-on, by operating near the resonance voltage [13] (i.e. at the transition between regions II and III of Fig. 2, rather than the normal operation at the transition between regions I and II).

Due to the small size of the quantum dot, Coulomb blockade (CB) effects play an important role in the resonant-tunneling regime, even at room temperature. The single-electron charging energy is roughly $U \sim 0.5$ eV, much larger than either k_BT or the width in energy Γ of the resonant state. (Here $k_BT \approx 0.025$ eV. The finite resonance width Γ arises because the localized state is degenerate in energy with the continuum of states in the NT leads, and we calculate that $\Gamma \approx 0.015$ eV). Since $U \gg \Gamma$, the device is in the CB regime, and the resonant level behaves in many ways as if truly localized.

We can include the most important effects of CB in our calculation in a relatively simple way. Because of the large value of U, there is no need to consider higher levels beyond the first CB resonance — they contribute negligible charge over the range of gate voltage of interest here. The first CB resonance occurs when the empty and singly-occupied states are degenerate, which is satisfied when the first one-electron level reaches the Fermi level. A localized electron has no "self-interaction", i.e. it does not feel its own electrostatic potential, so we calculate the potential in the quantum dot region treating the localized levels as empty. Outside of this region the states are extended, so we use the charge and potential calculated with the actual occupancies. Because of the strong spatial separation of the localized and extended states relevant for transport, this provides a reasonable approximation to a full self-interaction correction. We emphasize that this procedure is not a full many-body calculation of the transport. It is intended to give the position of the resonance. The actual conductance values are only suggestive. (The width of the peak in Fig. 2a corresponds to the gate voltage required to move the localized level by $\sim k_B T$ in energy, so it is probably fairly accurate.)

The band diagram of Fig. 2d and the conductance of Fig. 2a (solid line) were calculated using this approximation. To illustrate the importance of the CB effect, we also calculated the conductance without any correction for CB, as if $U \ll \Gamma$. The result is shown with a dotted line in Fig. 2a. The conductance peak is much sharper when CB is included, and is shifted to lower gate

voltages.

So far we have considered only the conductance at small source-drain voltage, where the system is close to equilibrium. To provide a more complete picture of the device characteristics, we calculated the current at larger voltage from [17]

$$I = \frac{4e}{h} \int P(E) [f(E) - f(E + eV_D)] dE , \qquad (2)$$

where V_D is the drain voltage (taking the source as "ground").

At any finite drain voltage, the system is not in equilibrium, so we adapt our calculation of the charge $\sigma(z)$ as described previously [5]. For large resistance (low transmission probability), the left and right sides of the device are each in approximate internal equilibrium, but with Fermi levels that differ by the drain voltage. We therefore calculate the charge using separate Fermi functions for the two regions. (In between, the Fermi level is deep in the bandgap, so the details of the cross-over from one side to the other have no effect on the charge or potential.) In the opposite limit of high transmission probability, we can approximate the electrons travelling from left to right as obeying the Fermi distribution of the left lead, while those moving from right to left obey the distribution of the right lead.

Figure 3 shows the current as a function of both drain and gate voltages. The device is a very effective transistor — for gate voltages corresponding to regions I and II of Fig. 2, the device exhibits high and low current respectively, with an abrupt transition between the two regimes. (For this figure, we use the low-transmission and high-transmission models for $V_G > 4$ V and $V_G < 3$ V, respectively. A smooth interpolation is used for intermediate gate voltages.)

At higher gate voltages, the resonant-tunneling peak (region III of Fig. 2a) appears as a ridge in Fig. 3a. At fixed gate voltage, with increasing drain voltage the current increases at first, because of the significant tunneling conductance. The current then reaches a maximum and decreases, as the resonant level moves into the bandgap of the drain, where there are no states available for tunneling. This behavior is shown in Fig. 3b. The gate voltage controls the energy of the resonant level, and so controls the position of the current maximum. Thus the device provides gated resonant tunneling and negative differential resistance.

An important characteristic of conventional transistors is that the current saturates with increasing drain voltage. Figure 4 shows that our NT device also displays current saturation. In conventional devices, the saturation is due to "pinch-off". The NT device, however, is ballistic, and the current is ultimately limited only by the number of available carriers in the leads. The dotted line in Fig. 4 shows the current in the limit of perfect transmission through the device. The actual current

calculated numerically is within about 20% of this ideal value. (For these calculations, we increased the length of the region treated self-consistently, because of electric field penetration into the contact region.)

Our results suggest that nanotube devices are excellent candidates for future nanoscale devices. In addition to their suitability as FETs, they can provide novel functionality such as room-temperature gated resonant tunneling. We anticipate that future NT device designs will provide further improvements in performance and additional new functionality.

F.L. acknowledges support from the NSERC of Canada and from the Office of Basic Energy Sicences, Division of Materials Sciences, U.S. Department of Energy under contract No. DE-AC04-94AL85000. Discussions with S. Datta are gratefully acknowledged.

- [1] C. Dekker, Physics Today 5, 22 (1999).
- [2] F. Léonard and J. Tersoff, Phys. Rev. Lett. 83, 5174 (1999);
- [3] F. Léonard and J. Tersoff, Phys. Rev. Lett. 84, 4693 (2000).
- [4] K. Esfarjani, A.A. Farajian, and Y. Kawazoe, Appl. Phys. Lett. 74, 79 (1999).
- [5] F. Léonard and J. Tersoff, Phys. Rev. Lett. 85, 4767 (2000).
- [6] A. Odintsov, Phys. Rev. Lett. 85, 150 (2000).
- [7] A. S. Maksimenko and G. Y. Slepyan, Phys. Rev. Lett. 84, 362 (2000).
- [8] H. Mehrez et al., Phys. Rev. Lett. 84, 2682 (2000).
- [9] S. J. Tans, A. R. M. Verschueren, and C. Dekker, Nature 393, 49 (1998).
- [10] R. Martel et al., Appl. Phys. Lett. **73**, 2447 (1998).
- [11] C. Zhou, J. Kong, and H. Dai, Appl. Phys. Lett. 76, 1597 (2000).
- [12] K. Tsukagoshi, B. W. Alphenaar, and H. Ago, Nature 401, 572 (1999).
- [13] P. Hylgaard and B. I. Lundqvist, Solid State Comm. 116, 569 (2000).
- [14] Gated resonant-tunneling devices have been fabricated in conventional materials, although a far more complicated structure is required — see Kolagunta et al., Appl. Phys. Lett. 69, 374 (1996), and references therein.
- [15] J. W. G. Wildöer et al., Nature 391, 59 (1998); T. W. Odom et al., Nature 391, 62 (1998).
- [16] H. Ago et al., J. Phys. Chem B 103, 8116 (1999); S. Suzuki, C. Bower, and Y. Watanabe, Appl. Phys. Lett. 76, 4007 (2000).
- [17] S. Datta, *Electronic transport in mesoscopic systems* (Cambridge University Press, Cambridge, 1995).
- [18] P. L. McEuen et al., Phys. Rev. Lett. 83 5098 (1999).

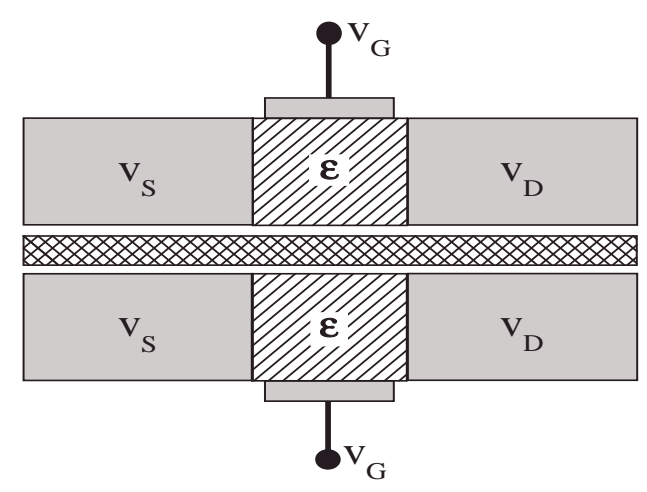


FIG. 1. Schematic cross-section of the nanotube device. Gray areas are the gate and the metallic source and drain contacts to the nanotube. Hatched areas represent the dielectric that surrounds the nanotube, and cross-hatched area is the nanotube. Source-drain separation is 10 nm; cylindrical gate has a radius of 10 nm.

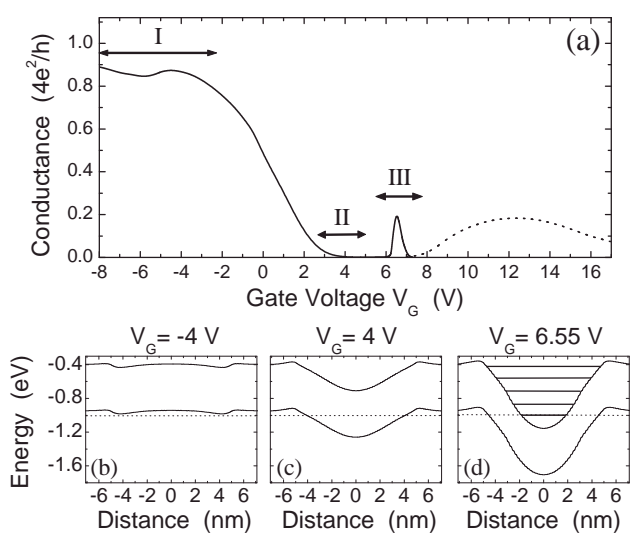


FIG. 2. (a) Conductance of the nanotube device at low bias. Solid line includes Coulomb-blockade effects, while dashed line is the result of a standard self-consistent calculation, as described in text. (b-d) Local valence and conduction band edges, from the self-consistent electrostatic potential, for gate voltage indicated. Dotted line is Fermi level. Due to the high metal workfunction, charge transfer between metal and NT leads to effective hole doping of the NT in the contacts, with the valence band edge 0.055 eV above the Fermi level. In (c), horizontal lines represent the single-particle energy levels due to quantum confinement.

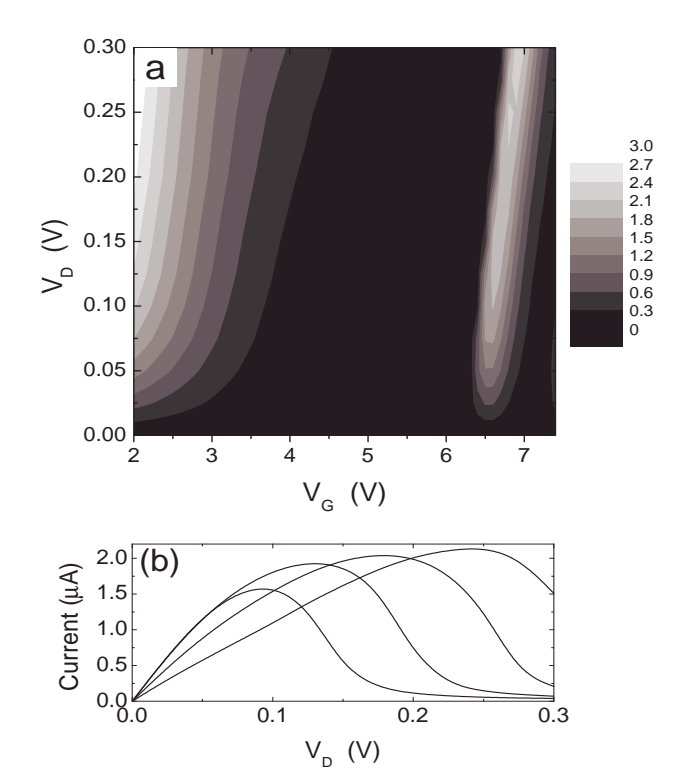


FIG. 3. (a) Current for the nanotube device (indicated by grey scale, in μ A) as a function of drain and gate voltages. (b) Current vs drain voltage for gate voltages (from left to right) V_G =6.5, 6.6, 6.7, and 6.8 V.

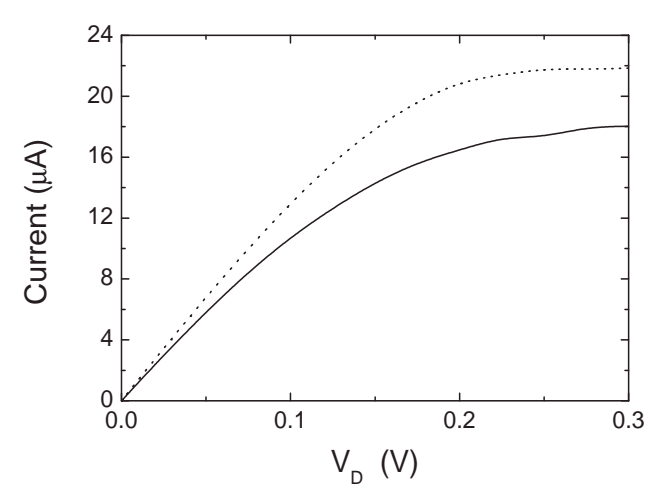


FIG. 4. Current as a function of drain voltage in the "on" regime $(V_G = -2V)$. Solid line is numerical result for the high transmission model. Dotted line is current in the limit of perfect transmission across the device, for comparison.